Nonlinear Compression of Intense Optical Pulses at 1.55 μm by Multiple Plate Continuum Generation

Chia-Lun Tsai, Yi-Hsun Tseng, An-Yuan Liang, Ming-Wei Lin, Shang-Da Yang, *Member, IEEE*, and Ming-Chang Chen, *Member, IEEE*

***Abstract*—Intense ultrashort laser pulses at 1.55 μm are generated by a home-built light source and compressed to 20 fs by multiple plate continuum (MPC) and Fourier pulse shaping. The entire system consists of three building blocks, responsible for seed generation, optical parametric chirped pulse amplification (OPCPA), and nonlinear compression. A commercial Yb:KGW amplifier pumps a difference frequency generator and an optical parametric amplifier (OPA) to generate 1 kHz, 44 fs, 10 μJ, carrier-envelope phase stable seed pulses at 1.55 μm. A grating–lens pair stretches the seed pulses to 50 ps by introducing a great amount of normal group delay dispersion (GDD). After that, the chirped pulse energy is boosted to 5 mJ by two OPA stages pumped by a commercial Nd:YAG amplifier (30 mJ, 85 ps). To compress the amplified pulses, a grating pair compressor providing an adequate amount of anomalous GDD is employed. The OPCPA system eventually delivers 3 mJ and 80 fs pulses, limited by the phase-matching bandwidth of nonlinear crystals. To further compress the pulse duration, pulses are sent to an MPC stage, which consisted of nine pieces of 200-μm-thick quartz plates. The OPCPA output spectrum is broadened by four times and compressed to 20 fs (3.6 carrier cycles) by a femtosecond Fourier-transform pulse shaper. The pulses are characterized by polarization gating cross-correlation frequency-resolved optical gating. Due to the high pondermotive force, an intense and long-wavelength laser system like this is useful in seeding a MeV-level electron accelerator and generating coherent soft X-ray high-harmonic generation.**

***Index Terms*—Optical parametric chirped pulse amplifier, pulse shaper, supercontinuum generation, ultrafast nonlinear optics.**

I. Introduction

HIGH-ENERGY ultrashort laser pulses have been accessible since the invention of chirped pulse amplification (CPA) [1]. The superior properties of Ti:Sapphire and Ytterbium-doped crystals lasing around 0.8 μm and 1 μm wavelengths make these lasers ideal for ultrafast science and technology. So far, the energies of Ti:Sapphire and Ytterbium-based laser pulses have reached hundreds of joules [2] and hundreds of milli-joules [3], respectively. These intense lasers are powerful tools in generating high-power terahertz radiation [4], laser plasma microcurrents [5], and coherent extreme ultra-violet (EUV) laser by high-harmonic generation (HHG) [6]. In the case of HHG, the resulting HHG source obtains high spatial and temporal resolution because its short wavelength and pulse duration. The short EUV wavelength supports a spatial resolution on the scale of tens of nanometers [7], which is attractive for the imaging of biological samples or nano-devices. The attosecond-scale EUV pulse width [8] can explore the fleeting electron dynamics in atoms, molecules, and materials via pump-probe experiments [9]. According to the semi-classical three-step model of HHG [10] and the model of cut-off photon energy in single atom [11], the maximum emitted photon energy $h\nu_{cutoff}$ can be formulated by

$$hv_{cutoff} = I_p + 3.17U_p \approx 3.17 I_L \lambda_L^2,$$

where I_p is the ionization potential of the target atom; U_p is the ponderomotive energy determined by the intensity I_L and wavelength λ_L of the driving laser. Furthermore, the phase matching cutoff scales [12] as

$$hv_{PM} \propto \lambda_L^{1.6} - \lambda_L^{1.7}.$$

These relations imply the general strategy of harvesting photons of higher energy, i.e., driving HHG with longer wavelengths. For example, the cutoff photon energy of HHG driven by Ti:Sapphire laser ($\lambda_L = 0.8\ \mu$m) is 120 eV in helium [11]. It increases to 170 eV when a Yb:CaF_2 driving laser ($\lambda_L = 1.03\ \mu$m) is used [13]. However, neither of them can generate photons in the range of water window (2.34∼4.4 nm, 280∼530 eV) [14]–[17] whose characteristics of high transmission for oxygen (and hydrogen) and high absorption for carbon (and nitrogen) are useful for *in-vivo* bio-nanoscopy and in-situ time-resolved pump-probe trial [18].

To red-shift, the driving laser wavelength, parametric down-conversion process such as OPA, can be employed [19], [20]. In OPA, pump power can be converted to signal and idler waves according to the conservation of energy and momentum. Down-converted pulses centered at signal and idler wavelengths of 1.44 and 1.8 μm (Ti:Sapphire pump) [21], 1.5 and 3.6 μm (Yb:KGW pump) [22], 1.5 and 3 μm (Yb:fiber pump) [23], 3.5 and 5.2 μm (Ho:YAG pump) [24], [25] or 2.8 and 7 μm (Ho:YLF pump) [26] have been reported. Although OPA enables a wide range of wavelength tuning, the effective gain bandwidth is limited

Manuscript received April 16, 2019; revised June 24, 2019; accepted July 15, 2019. Date of publication July 17, 2019; date of current version September 24, 2019. This work was supported by the Ministry of Science and Technology (MOST) Taiwan under Grants 104-2112-M-007-012-MY3, 105-2112-M-007-030-MY3, and 107-2112-M-007-006. *(Corresponding author: Chia-Lun Tsai.)*

The authors are with the Institute of Photonics Technologies, the Frontier Research Center on Fundamental and Applied Sciences of Matters, and the Institute of Nuclear Engineering and Science, National Tsing Hua University, Hsinchu 30013, Taiwan (e-mail: s102066805@m102.nthu.edu.tw; s102066508@m102.nthu.edu.tw; s103011252@m103.nthu.edu.tw; mwlin@mx.nthu.edu.tw; sdyang@ee.nthu.edu.tw; mingchang@mx.nthu.edu.tw).

Color versions of one or more of the figures in this paper are available online at http://ieeexplore.ieee.org.

Digital Object Identifier 10.1109/JLT.2019.2929287

by temporal walk-off between signal and idler pulses. In the case of OPCPA, the effective bandwidth is furthermore affected by temporal and wave vector overlapping between pump and seed pulses. These effects tend to narrow the parametric gain bandwidth such that the output pulse is longer than the front-end laser pulse [27]. For downstream applications preferring short duration and high intensity, it becomes highly desirable to compress the amplified pulses by spectral broadening and dispersion compensation to recover (or further shorten) the pulse width.

In terms of spectral broadening, supercontinuum generation is typically achieved by coupling the pulse into microstructured optical fiber [28], [29], gas-filled hollow-core fiber [30] bulk material [31], [32] or multiple pass cell [33]–[36]. However, the requirements of coupling and long interaction length make fibers subject to spectral distortion and power fluctuation induced by beam pointing drift. The energy scale of supercontinuum generation in bulk material is in the range of micro-joule. Multiple pass cell needs deliberate cavity design and precise optical alignment. In this regards, a new supercontinuum generation technique, multiple plate continuum (MPC) [37], was recently invented and has made rapid progress in the last few years. MPC has the advantages of easier optical alignment, lower economic cost, free from beam-pointing-induced issues, and capable of spatial multiplexing. It has been realized at pump wavelengths of 0.8 μm [37]–[41], 1 μm [42], [43], 1.5 μm [44] and 3.5 μm [45]. However, compressing the MPC pulse at 1.5 μm close to its transform limit (TL) remains undemonstrated.

In this work, we report four-fold nonlinear pulse compression by MPC and dispersion compensation at 1.5 μm. The driving laser system consisting of seed pulse generation (pumped by 100 μJ pulse from a commercial Yb:KGW amplifier) and OPCPA (pumped by 30 mJ pulse from a commercial Nd:YAG amplifier), delivers 1 kHz, 3 mJ, 80 fs pulses at 1.55 μm. Due to the lack of space for loose focusing, we only tap 0.7 mJ from the OPCPA for nonlinear pulse compression. The OPCPA output spectrum is substantially broadened by passing through 9 pieces of 200-μm-thick quartz plates and de-chirped by a Fourier pulse shaper, resulting in 20 fs (3.6-carrier-cycles) pulses at the output.

II. Front-End Laser System for MPC-Based Nonlinear Compression

The entire setup consists of three building blocks (Fig. 1): (1) generation of 10 μJ seed pulse at 1.5 μm by white-light generation (WLG) seeded difference frequency generation (DFG), OPA; (2) amplification of seed pulse to 3 mJ by OPCPA; (3) nonlinear broadening and compression of the 80 fs pulses to 20 fs by MPC and a Fourier pulse shaper. In this section, the first two building blocks will be discussed in detail, while the nonlinear pulse shortening scheme will be described in more detail in Section III.

We use a Yb:KGW laser system (Pharos, Light-conversion) comprising of a Kerr-lens mode-locked oscillator (OSC) and a chirped pulse regenerative amplifier (RA) to pump the seed pulse generator. The OSC operates at 76 MHz repetition rate and has two output beams. One of them (with 530 pJ energy) is seeded

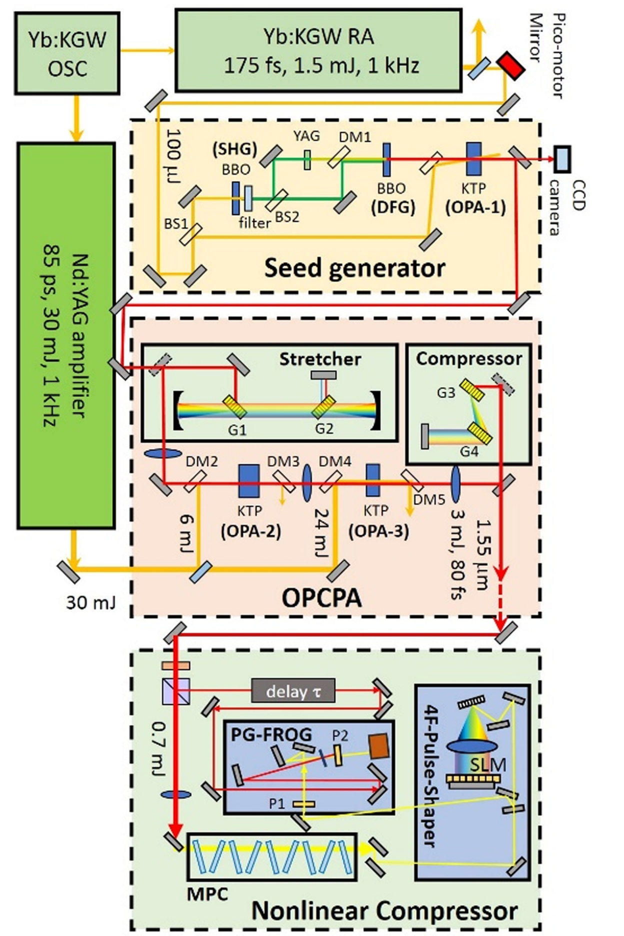

Fig. 1. Setup of the entire system. OSC, oscillator; RA, regenerative amplifier; OPA-#, optical parametric amplifier; BS#, beamsplitter, G#, transmission grating; P#, a linear polarizer, DM#, dichroic mirror; SLM, spatial light modulator.

to a Nd:YAG amplifier (EKSPLA) for energy enhancement to 30 mJ. Meanwhile, a 76 MHz signal from a photodiode (PD) in the OSC synchronizes Yb:KGW OSC and Nd:YAG amplifier electrically. The Nd:YAG amplifier can produce 1 kHz, 85 ps, 30 mJ pulses at 1.064 μm by using one regenerative amplifier (RA) and two power amplifiers (PAs). To improve the output beam quality, we add a spatial filter (consisting of two lenses and a pinhole of 610 μm diameter) between the two PAs. The output beam is 4.2 mm in diameter (defined by 1/e^2). The other beam of the Yb:KGW OSC seeds the Yb:KGW RA, where a Pockels cell selects pulses of 1 kHz repetition rate for amplification. The Yb:KGW RA emits 1 kHz, 170 fs, 1.5 mJ pulses at 1.03 μm with 4 mm beam diameter (1/e^2).

To generate passively carrier-envelope phase (CEP) stabilized seed at 1.55 μm, we only tap 100 μJ (7%) from the Yb:KGW RA for pumping. The 1.03 μm laser pulse is split into two paths by a beamsplitter (BS1). The weaker one (25 μJ) is spatially down-sized from 4 mm to 1.3 mm in diameter (1/e^2) to increase the conversion efficiency of second-harmonic generation (SHG) inside a 2-mm-thick BBO crystal (type I, $\theta = 23.4°$, $o_\omega + o_\omega \rightarrow e_{2\omega}$, $\varphi = 90°$). We use a filter to block fundamentals and only green pulses of 9 μJ (36% efficiency) at 515 nm are left. The green pulse is also divided into two paths by a beamsplitter (BS2). The first green pulse (2.7 μJ) drives a 10-mm-thick YAG crystal for WLG, then collinearly combined with the second green pulse (6.3 μJ) by a dichroic mirror DM1 to pump a 2-mm-thick BBO crystal (type I, $o_s+o_i \rightarrow e_p$, $\theta = 22.8°$, $\varphi = 90°$) for DFG at a peak intensity of 213 GW/cm^2. WLG operated under single filamentation, produces a stable and coherent spectrum spanning from 400 to 790 nm at -30 dB level. DFG between the pump (515 nm) and signal (771 nm, a slice of the WLG spectrum) originated from the common source will passively stabilize the CEP of the idler pulse (1.55 μm) [46]. Note that the collinear geometry is employed to suppress spatial chirp of the idler pulse.

To amplify the 1.55 μm pulse, the second 1.03 μm pulse (75 μJ) split from the output of Yb:KGW RA is spatially downsized from 4 mm to 2 mm before pumping a 6-mm-thick KTP crystal (type II, $e_s+o_i \rightarrow o_p$, x-z principal plane, $\theta = 48°$, $\varphi = 0°$) for OPA (OPA-1, Fig. 1). Pump (1.03 μm) and signal (1.55 μm) beams are crossed at 1.8° inside the KTP crystal, such that they can be spatially separated after amplification. By optimizing the phase-matching angle and the temporal and spatial overlapping, the 1.55 µm signal pulse is amplified to 10 µJ. The pulse duration measured by SHG-FROG is 44 fs, close to the transform-limited (TL) value of 40 fs.

To further increase the pulse energy, an OPCPA is built after the seed generator. In our setup, a Martinez (grating-lens pair) stretcher is used to temporally stretch the 44 fs, 1.55 μm input pulse by introducing a great amount of normal group delay dispersion (GDD). The stretcher is composed of two transmission gratings (940 gr/mm, 92% diffraction efficiency over 1525–1605 nm) and two identical curved mirrors (4 inches in diameter, the radius of curvature is 60 cm). The 1.55 µm beam is incident on the first grating (G1) at an angle of 47° to maximize the diffraction efficiency. After passing through the symmetric grating-lens pair, a flat mirror with a small tilt angle in the vertical direction reverses the beam path to eliminate spatial chirp. The residual spatial chirp caused by asymmetric orientations of the gratings (G1 and G2) is calibrated by inspecting whether the focused beam profile (f = 15 cm) after the stretcher is round or not. The double-pass configuration stretches the pulse from 44 fs to 50 ps (measured by intensity autocorrelation). Total throughput is 43% which comes from grating diffraction efficiency as well as from insufficient bandwidth of gratings.

The OPCPA amplifies the stretched pulse in two cascaded OPA stages. The first stage (OPA-2) uses a 10-mm-thick KTP crystal (type II, $e_s+o_i \rightarrow o_p$, x-z principal plane, $\theta = 45.5°$, $\varphi = 0°$). The pump beam profile on the KTP entrance surface is relayed from the end surface of Nd:YAG rod in the second PA of the Nd:YAG amplifier by a two-lens 4-f geometry, where a vacuum chamber is placed between the two lenses to avoid air breakdown that would destroy the beam quality. The first 1.064 μm pump beam (6 mJ) is spatially downsized to 0.63 mm in diameter (1/e^2) and exhibits a flat-top profile with 34 GW/cm^2 peak intensity. The flat-top beam profile is more robust against crystal damage induced by self-focusing and can provide a spatially uniform parametric gain for the signal pulse. Efficient OPA occurs after overlapping the pump and signal pulses temporally (with a delay stage) and spatially (by focusing the signal pulse to 0.39 mm in diameter in the KTP crystal), which can amplify the energy of the strongly up-chirped signal pulse (50 ps, 1.55 μm) by 125 times (from 4 μJ to 500 μJ) in OPA-2.

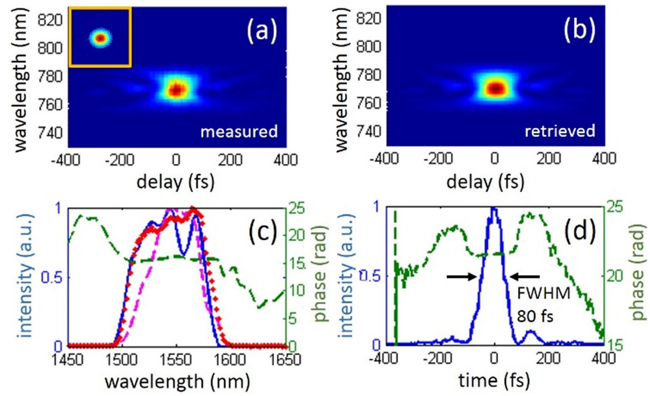

Fig. 2. Characterization of the OPCPA output pulse. (a) Measured and (b) retrieved SHG-FROG traces. A subplot in (a) is the focused beam profile taken by a silicon-based CCD camera by exploiting two-photon absorption effect. (c) Retrieved spectral intensity (blue solid) and spectral phase (green dashed). Spectra of OPA-2 (pink dashed) and OPA-3 (red dotted) are measured for reference. (d) Retrieved temporal intensity (blue solid) and phase (green dashed). FWHM is 80 fs.

The second stage (OPA-3) uses a thinner (6 mm) KTP crystal whose remaining parameters are the same as those used in OPA-2. Relay image is also carried out for the second 1.064 μm pump beam (24 mJ), while the beam diameter increases to 1.27 mm to maintain comparable peak intensity (31.6 GW/cm^2) under higher pump energy. The signal beam is recollimated to 1.44 mm in diameter by lenses and interacts with the pump beam collinearly. The signal pulse energy is amplified by a factor of 10 (from 500 μJ to 5 mJ) when all the conditions (phase-matching angle, temporal and spatial overlapping) are properly satisfied. Spectral broadening accompanied by amplification is observed in OPA-3, where the TL pulse width decreases from $\sim$100 fs to 78 fs [Fig. 2(c)]. This is primarily attributed to gain saturation, where photons around the spectral center (1.55 μm) experience smaller gain than those at the spectral wings. The amplified pulse (50 ps, 5 mJ, 1.55 μm) is then de-chirped by a grating pair compressor, which can introduce quadratic and cubic spectral phase coefficients of the same magnitude but in opposite signs with those of the Martinez stretcher. This is possible if the stretcher and compressor are built with identical parameters, including groove density, grating distance, and incident angle. To prevent self-phase modulation and self-focusing, the thickness of the grating substrate is as thin as 675 μm to avoid a high B-integral. By adjusting the incident angle and separation between the gratings, we are able to compress the pulse to 80 fs (measured by SHG-FROG, see Fig. 2) with 3 mJ energy. The separation between the two compressor gratings is slightly less than that of the stretcher due to GDD induced by the nonlinear crystals.

Since the output pulse energy of the entire system highly depends on the beam pointing of front-end lasers, the mirror mounts between the Yb:KGW RA and seed generator are being

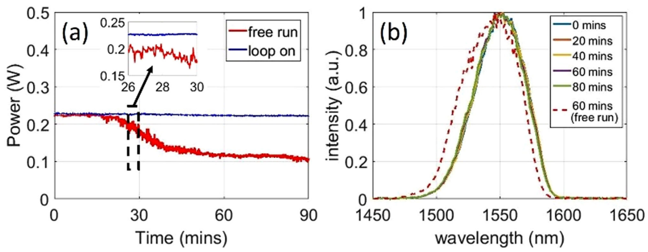

Fig. 3. (a) Power with (blue) and without (red) feedback loop control of OPA-2. Inset: power fluctuation within 4 minutes. (b) Power spectra were taken at 0, 20, 40, 60, 80 minutes with (solid lines) and without (dashed lines) feedback control.

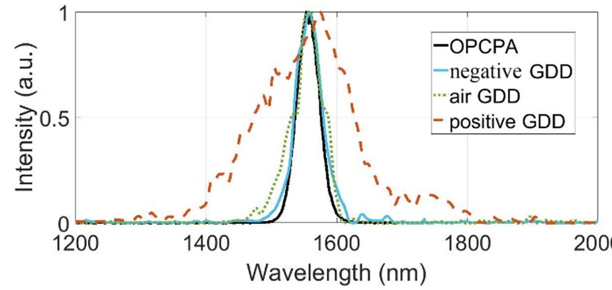

Fig. 4. MPC spectra obtained by input pulses with positive (red-dashed), air (green-dotted), and negative (blue-solid) GDD. The spectrum of OPCPA is also plotted as reference (black-solid).

driven by two pico-motors such that the laser beam pointing can be independently controlled in x- and y-directions. A CCD camera is placed at the output of OPA-1 to record the beam profile in real time. By confining the center of mass of the beam profile within a small area ($\sim$6.6 $\times$ 6.6 μm^2) using a feedback software routine, the beam pointing direction is locked within 1.76 μrad. In this way, the output powers and spectra of the seed generator and the subsequent OPCPA are greatly stabilized. In the free running mode, the output power of OPA-2 drops by 47% in 90 minutes [Fig. 3(a)] and the largest fluctuation occurs by 4.7% within a time interval of 4 minutes [inset, Fig. 3(a)]. When the feedback loop is on, it only drops by 1.4% in 90 minutes and fluctuates by 0.4% within 4 minutes. The output power spectrum of OPA-2 is also greatly stabilized by the feedback loop. No noticeable change of spectral shape is observed in 80 minutes when the loop is on, while it can change wildly in the free running mode [Fig. 3(b)]. The stability performance of OPA-3 exhibits similarly. The shot-to-shot fluctuation (standard deviation over mean in 200 shots) is 1.74%, while the long term fluctuation is 0.37% (recorded over 90 minutes) with the feedback loop. A laser source of such stability would be necessary to drive the down-stream nonlinear pulse compressor.

As to the CEP issue, our originated 1550 nm seed source from DFG is CEP stabilized. However, due to the effects of grating stretcher and compressor, CEP is deteriorated and shifted randomly [47]. We expect that by using volume Bragg gratings (VBG) as components to stretch and compress pulses in OPCPA [48], and CEP would be sustained as the same of originated condition.

III. Nonlinear Pulse Compression by MPC and Femtosecond Fourier Pulse Shaper

Since stronger peak intensity and shorter duration of driving laser pulse contribute to higher photon energy and fewer attosecond bursts per driving shot in HHG, further compressing the 80 fs OPCPA pulse while preserving most of the energy is practically useful for generating isolated attosecond pulse in the water window regime. It can be realized in two further steps: (1) spectral broadening by nonlinear optical effects; (2) phase equalization for all frequency components. As indicated in Section I, all-solid-state MPC method is chosen to substantially broaden the spectrum for the sake of easier optical alignment, immunity to beam-pointing induced spectral distortion (compared to using hollow core fibers), improving beam quality, and capability of spatial multiplexing. Instead of using sophisticated capillary or multiple pass cell, MPC only needs a couple of thin plates as the nonlinear media. The thickness of plates can vary from 50 μm to 1 mm, depending on the damage threshold of material and the desire nonlinear phase shift induced in each plate.

Our nonlinear pulse compressor contains a MPC stage and a femtosecond Fourier pulse shaper (Fig. 1). The optical beam from the OPCPA is divided into two paths to drive MPC and serve as the reference of PG-XFROG pulse measurement system. Due to the lack of space for loose focusing and to avoid damaging the spatial light modulator in the pulse shaper, we only tap 700 μJ from the OPCPA output for MPC. We focus the laser beam into the MPC stage by a lens (f = 0.5 m) such that the spot size on the first plate is 190 μm in diameter. The first plate (200-μm-thick quartz) is placed at the focal plane, where the peak intensity is $\sim 5.4 \times 10^{13}\ \mathrm{W/cm^2}$. Spectral broadening and self-focusing occur inside the plate simultaneously, and the beam leaves the plate before it gets damaged by the increased intensity. We control the B-integral is $\sim\pi$ in each plate. The second plate is placed such that the light intensity returns to the incident level due to diffraction in the air. This process continues until the spectrum does not broaden anymore mainly due to the decreasing of intensity at focal plane due to the conical emission which comes from the strong Kerr lensing effect, inducing an unwanted abbreviation in wavefront.

In our experiment, we firstly investigate the impact of input pulse chirp on the spectral broadening in MPC at 1.55 μm. Pulses with different chirp will influence nonlinear pulse broadening [49], [50]. Figure 4 displays the MPC spectra (9 pieces of 200-μm-thick quartz plates) obtained by 700 μJ pulses with positive (red-dashed), air (green-dotted), and negative (blue-solid) group delay dispersion (GDD) controlled by the compressor of the OPCPA, respectively. The quartz plate is made with z-cut and placed with Brewster's angle to optimize the transmission rate. The polarization of the beam is p-wave. Chirp rate of input pulses is measured with PG-XFROG after beam passing through focusing lens but with no quartz plates inserted into the beam. Pulses with positive GDD causes significant spectral broadening, whereas the input pulse with negative GDD performs nearly no spectral broadening after passing through multiple plates. It

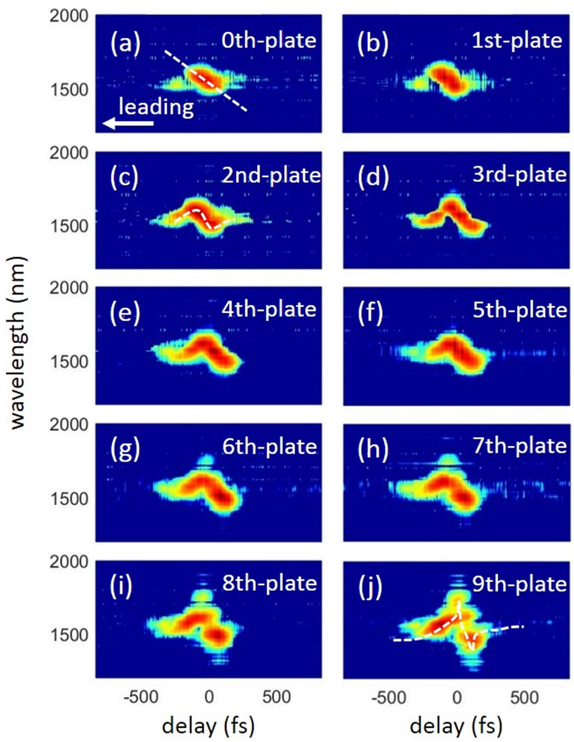

Fig. 5. Normalized PG-XFROG traces of MPC pulses after different numbers of plates with identical input laser intensity.

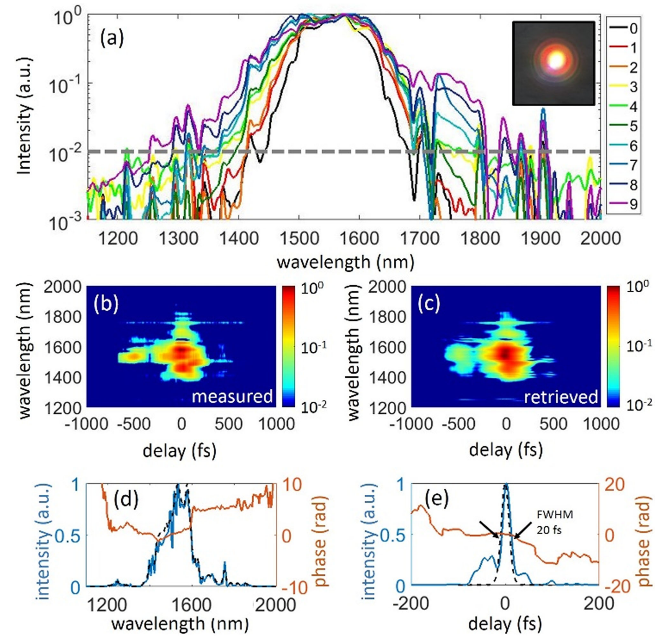

Fig. 6. (a) MPC spectra after insertion of different numbers of 200 μm-thick quartz plates. Inset represents the beam profile of 1.55 μm MPC taken by a silicon-based CCD camera. (b) Measured and (c) retrieved PG-XFROG traces of the de-chirped MPC pulse. Intensity (blue) and phase (red) profiles of retrieved MPC pulse displayed in (d) frequency and (e) time domains. The power spectrum acquired by a monochromator and TL temporal intensity is shown in black dotted in (d) and (e) for reference.

is attributed to the fact that quartz exhibits anomalous dispersion at 1.55 μm, which would suppress the temporal stretching of an up-chirped input pulse. As a result, the pulse can maintain high peak intensity for a longer propagation distance and thus induce stronger spectral broadening effect during this process. We take further process by using the broadest condition of MPC (Fig. 4, red-dotted line). The separations of 9 plates are 3.5, 1.5, 1.8, 1.4, 1.5, 1.1, 1.1, and 0.9 cm.

At the exit of each plate, we record a PG-XFROG trace [Figs. 5(a)$\sim$(j)] by using 80 fs reference pulse from the OPCPA output and a commercial spectrometer (RED-Wave-NIRX, Stellarnet). Figure 5 shows that due to self-phase modulation (SPM) both new red- and blue-shifting wavelength components are created, respectively, during the first five plates. Then, redshift becomes more obvious from the 6$^{\text{th}}$ plate onward. As a result, the PG-XFROG trace appears to be in the shape of “N.” We also observed the pulse chirp around time zero in Fig. 5(j) becomes much smaller than in Fig. 5(a) due to the anomalous dispersion in fused silica plates. The final MPC spectrum extends from 1.25 μm to 1.9 μm at -20 dB level [red, Fig. 6(a)], sufficient to support 19.7 fs (3.8 carrier cycles) TL pulse. Unlike the MPC experiments in 800 nm [37] and 1030 nm [42] with a signature long blue tail attributed to self-steepening effect, our current MPC spectrum extends more symmetrically, also implying that SPM plays the main role in the spectral broadening. The total transmission is 53.6%, where the major loss comes from the loss of the conical diffracting rings. The beam profile of 1.55 mm MPC is taken by a silicon-based CCD camera. The noisy MPC spectra with lots of peaks on the slopes is due to a low spectral resolution and a low dynamic range in each pixel. We have used another spectrometer (Sol 1.7, B&W tek.) to obtain smooth spectra. However, limited to its spectral range of 0.9$\sim$1.7 μm, we finally choose this spectrometer with a larger spectral range but a lower dynamic range and a spectral resolution for this experiment.

Pulses after MPC stage are sent into a Fourier pulse shaper to correct the spectral phase (Fig. 1). The pulse shaper consists of a 4-f zero dispersion stretcher and a liquid crystal spatial light modulator (SLM) placed on the focal plane. Since the SLM pixels can only introduce a phase shift up to 1.6π per passage at 1.8 μm wavelength, we configure our pulse shaper in reflective type to double the accumulated phase shift in the SLM. By choosing gratings of 400 gr/mm, the 4-f zero dispersion stretcher can disperse wavelengths from 1.14 μm to 1.95 μm over a 64 mm window on the focal plane, essentially covering the entire MPC spectrum (1.25–1.9 μm at -20 dB level). Each liquid crystal pixel of the SLM is 100 μm wide, corresponding to 1.67 nm bandwidth at 1.55 μm. The relation between the phase shift and the driving electric signal of the SLM is calibrated by a two-channel (1310 nm, 1550 nm) CW laser, a wavelength tunable (1530-1610 nm) CW laser (eTL-2100, EZconn), and a wavelength tunable (1550-3370 nm) mid-infrared CW laser (ICOPO-TB-α, HC-Photonics) at wavelengths of 1310 nm, 1500 nm, 1550 nm, 1600 nm, 1650 nm, 1700 nm, 1750 nm, 1800 nm, 1850 nm, 1900 nm. The spectral phase function of the

MPC pulse is characterized by PG-XFROG with a home-made least square generalized projection phase retrieval engine and fed to the SLM for compensation.

A loop of measurement-and-compensation is conducted until all the frequency components are nearly in-phase. Figures 6(b) and 6(c) illustrate the measured and retrieved PG-XFROG traces of the de-chirped MPC pulse. The retrieved temporal intensity [blue solid, Fig. 6(e)] spans 20 fs in FWHM, very close to the TL value of 19.7 fs [black dashed, Fig. 6(e)]. However, the residual spectral phase [red solid, Fig. 6(d)] causes non-negligible pedestal in the time domain (60% energy still in the main pulse). The pedestal will cause plasma which influences the phase-matching and the conversion efficiency of HHG. Because of the low spectral resolution of our current PG-XFROG measurement (9 nm) and the pulse shaper based compressor (1.67 nm in each pixel), we cannot observe and further compensate the fine spectral distortion of the pulses of MPC. In other words, the pulse shaper has an uncertainty of 9 nm due to the spectrometer. This residual high order phase causes the unwanted side lobes [51]. Furthermore, the uncoated SLM used in this experiment exhibits low transmission from 1600 to 2000 nm, which tends to narrow MPC bandwidth. Better pulse shapes would require an upgraded measurement and a high resolution shaper, or broadband chirped mirrors for dechirping. Note that compared to the self-compression method [35], our approach can handle mJ-level pulses and gain enough bandwidth in a limited space. Furthermore, by separating the spectral broadening and the phase compensation into two different setups, we can control the nonlinear bandwidth and the spectral phase independently.

IV. Conclusion

We built an OPCPA system delivering 1 kHz, 3 mJ, 80 fs pulses at 1.55 μm, pumped by a 1 kHz, 30 mJ, 80 ps Nd:YAG laser amplifier. The CEP-stable seed pulses at 1.55 μm are generated by DFG and OPA pumped by a Yb:KGW amplifier. Tapping 0.7 mJ per pulse from the OPCPA, the spectrum is broadened by four times (spanning from 1.25 μm to 1.9 μm at -20 dB) when using MPC, 9 strategically placed 200-μm-thick quartz plates. The residual spectral phase is compensated by a Fourier pulse shaper, compressing the temporal intensity profile close to its transform limit (20 fs versus 19.7 fs). Laser pulse energy up-scaling is possible by using a looser lens focusing on MPC and chirp mirrors for the dispersion compensation. Shorter few-cycle pulses can be accomplished by introducing an additional MPC and dispersion compensation stage. Upcoming applications of this laser are expected useful for generating coherent light source in the water window or soft-X-ray [52], intense THz generation by optical rectification [53] or laser-driven electron acceleration in plasma [54], [55].

Acknowledgment

The authors would like to thank Dr. Chih-Hsuan Lu and Prof. A. H. Kung for the discussion on MPC. Chia-Lun Tsai would like to thank Prof. Szu-Yuan Chen for lending SLM, Prof. Yu-Chueh Hung for lending 0.9–2.5 μm spectrometer, Prof. Chang-Hua Liu for lending tunable CW mid-infrared laser, Prof. Wei-Wei Hsiang for the discussion on mid-infrared lasers, Prof. Yuan-Yao Lin for the discussion on 1.55 μm in material, Dr. Chien-Chung Lee for the CEP discussion, Hsiang-Nan Cheng for the EKSPLA laser discussion, and Chung-Lo Chen, Chia-Hao Guo, and Jhan-You Guo for their short-term help.

References

[1] D. Strickland and G. Mourou, "Compression of amplified chirped optical pulses," *Opt. Commun.*, vol. 56, no. 3, pp. 219–221, Dec. 1985.
[2] Y. Chu *et al.*, "High-energy large-aperture Ti:sapphire amplifier for 5 PW laser pulses," *Opt. Lett.*, vol. 40, no. 21, pp. 5011–5014, Nov. 2015.
[3] E. Kaksis, G. Almási, J. A. Fülöp, A. Pugžlys, A. Baltuška, and G. Andriukaitis, "110-mJ 225-fs cryogenically cooled Yb:CaF_2 multipass amplifier," *Opt. Express*, vol. 24, no. 25, pp. 28915–28922, Dec. 2016.
[4] J. A. Fülöp *et al.*, "Highly efficient scalable monolithic semiconductor terahertz pulse source," *Optica*, vol. 3, no. 10, pp. 1075–1078, Oct. 2016.
[5] K. Y. Kim, J. H. Glownia, A. J. Taylor, and G. Rodriguez, "Terahertz emission from ultrafast ionizing air in symmetry-broken laser fields," *Opt. Express*, vol. 15, no. 8, pp. 4577–4584, Apr. 2007.
[6] M. Ferray, A. L'Huillier, X. F. Li, L. A. Lompre, G. Mainfray, and C. Manu, "Multiple-harmonic conversion of 1064 nm radiation in rare gases," *J. Phys. B, At. Mol. Opt. Phys.*, vol. 21, no. 3, pp. L31–L35, Nov. 1987.
[7] D. F. Gardner *et al.*, "Subwavelength coherent imaging of periodic samples using a 13.5 nm tabletop high-harmonic light source," *Nature Photon.*, vol. 11, pp. 259–263, Mar. 2017.
[8] F. Silva, S. M. Teichmann, S. L. Cousin, M. Hemmer, and J. Biegert, "Spatiotemporal isolation of attosecond soft X-ray pulses in the water window," *Nature Commun.*, vol. 6, no. 6611, pp. 1–6, Mar. 2015.
[9] M. Qin and X. Zhu, "Molecular orbital imaging for partially aligned molecules," *Opt. Laser Technol.*, vol. 87, pp. 79–86, Jan. 2017.
[10] P. B. Corkum, "Plasma perspective on strong field multiphoton ionization," *Phys. Rev. Lett.*, vol. 71, no. 13, pp. 1994–1997, Sep. 1993.
[11] T. Popmintchev, M. C. Chen, P. Arpin, M. M. Murnane, and H. C. Kapteyn, "The attosecond nonlinear optics of bright coherent X-ray generation," *Nature Photon.*, vol. 4, pp. 822–832, Nov. 2010.
[12] T. Popmintchev *et al.*, "Phase matching of high harmonic generation in the soft and hard X-ray regions of the spectrum," *Proc. Nat. Acad. Sci. USA*, vol. 106, no. 26, pp. 10516–10521, Jun. 2009.
[13] T. Balčiūnas *et al.*, "Efficient 170 eV source directly driven by an Yb laser amplifier," in *Proc. Eur. Conf. Lasers Electro-Opt.*, Munich, Germany, Jun. 2017.
[14] T. Popmintchev *et al.*, "Bright coherent ultrahigh harmonics in the keV X-ray regime from mid-infrared femtosecond lasers," *Science*, vol. 336, no. 6086, pp. 1287–1291, Jun. 2012.
[15] M. C. Chen *et al.*, "Bright, coherent, ultrafast soft X-ray harmonics spanning the water window from a tabletop light source," *Phys. Rev. Lett.*, vol. 105, no. 17, pp. 173901–173904, Oct. 2010.
[16] N. Ishii, K. Kaneshima, K. Kitano, T. Kanai, S. Watanabe, and J. Itatani, "Carrier-envelope phase-dependent high harmonic generation in the water window using few-cycle infrared pulses," *Nature Commun.*, vol. 5, no. 3331, pp. 1–6, Feb. 2014.
[17] S. M. Teichmann, F. Silva, S. L. Cousin, M. Hemmer, and J. Biegert, "0.5-keV soft X-ray attosecond continua," *Nature Commun.*, vol. 7, no. 11493, pp. 1–6, May 2016.
[18] P. Wachulak *et al.*, "Bioimaging using full field and contact EUV and SXR microscopes with nanometer spatial resolution," *Appl. Sci.*, vol. 7, no. 6, pp. 548–560, May 2017.
[19] J. A. Giordmaine and R. C. Miller, "Tunable coherent parametric oscillation in $LiNbO_3$ at optical frequencies," *Phys. Rev. Lett.*, vol. 14, no. 24, pp. 973–976, Jun. 1965.
[20] F. Rotermund, V. Petrov, F. Noack, L. Isaenko, A. Yelisseyev, and S. Lobanov, "Optical parametric generation of femtosecond pulses up to 9 μm with $LiInS_2$ pumped at 800 nm," *Appl. Phys. Lett.*, vol. 78, no. 18, pp. 2623–2625, Apr. 2001.
[21] C. Li *et al.*, "Generation of carrier-envelope phase stabilized intense 1.5 cycle pulses at 1.75 μm," *Opt. Express*, vol. 19, no. 7, pp. 6783–6789, Mar. 2011.
[22] O. D. Mücke *et al.*, "Self-compression of millijoule 1.5 μm pulses," *Opt. Lett.*, vol. 34, no. 16, pp. 2498–2500, Aug. 2009.
[23] P. Rigaud *et al.*, "Supercontinuum-seeded few-cycle mid-infrared OPCPA system," *Opt. Express*, vol. 24, no. 23, pp. 26494–26502, Nov. 2016.

[24] T. Kanai *et al.*, “Parametric amplification of 100 fs mid-infrared pulses in $ZnGeP_2$ driven by a Ho:YAG chirped-pulse amplifier,” *Opt. Lett.*, vol. 42, no. 4, pp. 683–686, Feb. 2017.
[25] M. Bock, L. V. Grafenstein, U. Griebner, and T. Elsaesser, “Generation of millijoule few-cycle pulses at 5 μm by indirect spectral shaping of the idler in an optical parametric chirped pulse amplifier,” *J. Opt. Soc. Amer. B*, vol. 35, no. 12, pp. C18–C24, Dec. 2018.
[26] D. Sanchez *et al.*, “7 μm, ultrafast, sub-millijoule-level mid-infrared optical parametric chirped pulse amplifier pumped at 2 μm,” *Optica*, vol. 3, no. 2, pp. 147–150, Feb. 2016.
[27] G. Cerullo and S. D. Silvestri, “Ultrafast optical parametric amplifiers,” *Rev. Sci. Instrum.*, vol. 74, no. 1, pp. 1–18, Jul. 2003.
[28] J. M. Dudley, G. Genty, and S. Coen, “Supercontinuum generation in photonic crystal fiber,” *Rev. Modern Phys.*, vol. 78, no. 4, pp. 1135–1184, Oct. 2006.
[29] J. H. V. Price *et al.*, “Supercontinuum generation in non-silica fibers,” *Opt. Fiber Technol.*, vol. 18, no. 5, pp. 327–344, Sep. 2012.
[30] B. Schenkel *et al.*, “Generation of 3.8-fs pulses from adaptive compression of a cascaded hollow fiber supercontinuum,” *Opt. Lett.*, vol. 28, no. 20, pp. 1987–1989, Oct. 2003.
[31] A. Dubietis, G. Tamošauskas, R. Šuminas, V. Jukna, and A. Couairon, “Ultrafast supercontinuum generation in bulk condensed media,” *Lithuanian J. Phys.*, vol. 57, no. 3, pp. 113–157, Jun. 2017.
[32] M. Seidel, G. Arisholm, J. Brons, V. Pervak, and O. Pronin, “All solid-state spectral broadening: An average and peak power scalable method for compression of ultrashort pulses,” *Opt. Express*, vol. 24, no. 9, pp. 9412–9428, Apr. 2016.
[33] M. Hanna *et al.*, “Nonlinear temporal compression in multipass cells: Theory,” *J. Opt. Soc. Amer. B*, vol. 34, no. 7, pp. 1340–1347, Jun. 2017.
[34] K. Fritsch, M. Poetzlberger, V. Pervak, J. Brons, and O. Pronin, “All-solid-state multipass spectral broadening to sub-20 fs,” *Opt. Lett.*, vol. 43, no. 19, pp. 4643–4646, Oct. 2018.
[35] G. Jargot *et al.*, “Self-compression in a multipass cell,” *Opt. Lett.*, vol. 43, no. 22, pp. 5643–5646, Nov. 2018.
[36] J. Schulte, T. Sartorius, J. Weitenberg, A. Vernaleken, and P. Russbueldt, “Nonlinear pulse compression in a multi-pass cell,” *Opt. Lett.*, vol. 41, no. 19, pp. 4511–4514, Aug. 2016.
[37] C. H. Lu *et al.*, “Generation of intense supercontinuum in condensed media,” *Optica*, vol. 1, no. 6, pp. 400–406, Dec. 2014.
[38] P. C. Huang *et al.*, “Polarization control of isolated high-harmonic pulses,” *Nature Photon.*, vol. 12, pp. 349–354, Apr. 2018.
[39] P. He *et al.*, “High-efficiency supercontinuum generation in solid thin plates at 0.1 TW level,” *Opt. Lett.*, vol. 42, no. 3, pp. 474–477, Feb. 2017.
[40] C. H. Lu, T. Witting, A. Husakou, M. J. J. Vrakking, A. H. Kung, and F. J. Furch, “Sub-4 fs laser pulses at high average power and high repetition rate from an all-solid-state setup,” *Opt. Express*, vol. 26, no. 7, pp. 8941–8956, Apr. 2018.
[41] J. E. Beetar, S. G. Mirzaei, and M. Chini, “Spectral broadening and pulse compression of a 400 μJ, 20 W Yb:KGW laser using a multi-plate medium,” *Appl. Phys. Lett.*, vol. 112, no. 5, Jan. 2018, Art. no. 051102.
[42] C. H. Lu *et al.*, “Greater than 50 times compression of 1030 nm Yb:KGW laser pulses to single-cycle duration,” *Opt. Express*, vol. 27, no. 11, pp. 15638–15648, May 2019.
[43] N. Ishii, P. Xia, T. Kanai, and J. Itatani, “Optical parametric amplification of carrier-envelope phase-stabilized mid-infrared pulses generated by intra-pulse difference frequency generation,” *Opt. Express*, vol. 27, no. 8. pp. 11447–11454, Apr. 2019.
[44] R. Budriūnas, D. Kučinskas, and A. Varanavičius, “High-energy continuum generation in an array of thin plates pumped by tunable femtosecond IR pulses,” *Appl. Phys. B*, vol. 123, no. 7, pp. 1–9, Jul. 2017.
[45] F. Lu, P. Xia, Y. Matsumoto, T. Kanai, N. Ishii, and J. Itatani, “Generation of sub-two-cycle CEP-stable optical pulses at 3.5 μm from a KTA-based optical parametric amplifier with multiple-plate compression,” *Opt. Lett.*, vol. 43, no. 11, pp. 2720–2723, Jun. 2018.
[46] A. Baltuška, T. Fuji, and T. Kobayashi, “Controlling the carrier-envelope phase of ultrashort light pulses with optical parametric amplifier,” *Phys. Rev. Lett.*, vol. 88, no. 13, Apr. 2002, Art. no. 133901.
[47] Z. Chang, “Carrier-envelope phase shift caused by grating-based stretchers and compressors,” *Appl. Opt.*, vol. 45, no. 32, pp. 8350–8353, Nov. 2006.
[48] K. H. Hong *et al.*, “High-energy, phase-stable, ultrabroadband kHz OPCPA at 2.1 μm pumped by a picosecond cryogenic Yb:YAG laser,” *Opt. Express*, vol. 19, no. 16, pp. 15538–15548, Aug. 2011.
[49] R. H. Stolen and C. Lin, “Self-phase-modulation in silica optical fibers,” *Phys. Rev. A*, vol. 17, no. 4, pp. 1448–1453, Apr. 1978.
[50] S. C. Pinault and M. J. Potasek, “Frequency broadening by self-phase modulation in optical fibers,” *J. Opt. Soc. Amer. B*, vol. 2, no. 8, pp. 1318–1319, Aug. 1985.
[51] A. M. Weiner, D. E. Leaird, J. S. Patel, and J. R. Wullert, “Programmable shaping of femtosecond optical pulses by use of 128-element liquid crystal phase modulator,” *IEEE J. Quantum Electron.*, vol. 28, no. 4, pp. 908–920, Apr. 1992.
[52] W. Chao, B. D. Harteneck, J. A. Liddle, E. H. Anderson, and D. T. Attwood, “Soft X-ray microscopy at a spatial resolution better than 15 nm,” *Nature*, vol. 435, no. 7046, pp. 1210–1213, Jun. 2005.
[53] F. Meyer *et al.*, “Optical rectification of a 100 W average power mode-locked thin-disk oscillator,” *Opt. Lett.*, vol. 43, no. 24, pp. 5909–5912, Dec. 2018.
[54] T. Tajima and J. M. Dawson, “Laser electron accelerator,” *Phys. Rev. Lett.*, vol. 43, no. 4, pp. 267–270, Jul. 1979.
[55] F. Salehi *et al.*, “MeV electron acceleration at 1 kHz with $<$10 mJ laser pulses,” *Opt. Lett.*, vol. 42, no. 2, pp. 215–218, Jan. 2017.

Chia-Lun Tsai received the B.S. degree in electrical engineering from National Tsing Hua University, Hsinchu, Taiwan, in 2010, and the M.S. degree from the Institute of Photonics Technologies, National Tsing Hua University, in 2013, where he is currently working toward the Ph.D. degree.

His works are mainly on femtosecond optical parametric chirp pulse amplifier, and nonlinear pulse compression. His research interests include optical parametric amplifiers, femtosecond pulse measurement and ultrafast fiber (and thin-disk) oscillators, and solid-state amplifiers.

Yi-Hsun Tseng received the B.S. degree in electrical engineering from National Tsing Hua University, Hsinchu, Taiwan, in 2013 and the M.S. degree from the Institute of Photonics Technologies, National Tsing Hua University, in 2017. He is currently a high school teacher responsible for scientific teaching. His research interests focus on optical parametric chirp pulse amplifier, ultrafast pulse measurement, and extreme ultra-violet high-harmonic generation.

An-Yuan Liang received the B.S. degree in engineering and system science from National Tsing Hua University, Hsinchu, Taiwan, in 2018, where she is currently working toward the M.S. degree at the Institute of Photonics Technologies. Her research interests focus on ultrafast thin-disk oscillators and ultrafast pulse measurement.

Ming-Wei Lin received the B.S. and M.S. degrees in engineering and system science from National Tsing Hua University, Hsinchu, Taiwan, in 2002 and 2004, respectively, and the Ph.D. degree in nuclear engineering from the Pennsylvania State University, State College, PA, USA, in 2015. Since 2016, he has been an Assistant Professor with National Tsing Hua University, Hsinchu, Taiwan, from which he continues to develop himself with a variety of research topics, ranging from ultrafast laser technologies, plasma particle-in-cell simulation, laser-driven particle acceleration, and radiation detection of high-energy prompt gamma rays and neutrons.

Shang-Da Yang (S'01–M'05) was born in Chiayi, Taiwan, in 1975. He received the B.S. degree in electrical engineering from National Tsing Hua University, Hsinchu, Taiwan, in 1997, the M.S. degree in electro-optical engineering from National Taiwan University, Taipei, Taiwan, in 1999, and the Ph.D. degree from the School of Electrical and Computer Engineering, Purdue University, West Lafayette, IN, USA, in 2005, respectively. In 2005, he joined National Tsing Hua University, and is currently a Full Professor. In 2011, he was a Visiting Professor with the Joint Institute for Laboratory Astrophysics, University of Colorado at Boulder, Boulder, CO, USA. His research interests include synthesis and characterizations of optical arbitrary waveforms, quasi-phase matching engineering, femtosecond fiber oscillators, and solid-state supercontinuum generation.

Prof. Yang is the recipient of the RiTEK Young Investigator Medal of the Optical Engineering Society of the Republic of China in 2007.

Ming-Chang Chen (M'19) received the B.S. and M.S. degrees, respectively, from National Tsing Hua University (NTHU) and National Chiao Tung University (NCTU), Hsinchu, Taiwan, and the Ph.D. degree in physics from the JILA, University of Colorado at Boulder, Boulder, CO, USA, in 2012. Since 2013, he has been with the Institute of Photonics Technologies and Electrical Engineering, NTHU. Currently, he focuses his research on demonstrating novel techniques for generation and characterization of short-duration light pulses in the deep-ultraviolet and soft X-ray regions of the spectrum, and its applications in measuring quantum dynamics in atoms, molecules, and novel materials.